Satellite Navigation
https://satellite-navigation.springeropen.com/

ORIGINAL ARTICLE

Open Access

High-precision GPS orbit determination by integrating the measurements from regional ground stations and LEO onboard receivers

Kai Li[1], Chengpan Tang[1*], Shanshi Zhou[1], Xiaogong Hu[1] and Xuhua Zhou[1]

Abstract

High-precision Global Navigation Satellite System (GNSS) orbit and clock products are crucial for precise applications. An evenly distributed global network enables continuous tracking for GNSS satellites, while a regional network may result in tracking gaps in the areas where monitoring stations are not deployed. This also means that the orbit determination accuracy based on a regional network is not comparable to that with a global network. Integrating the measurements from regional ground stations and Low Earth Orbit (LEO) satellites onboard receivers is a potential approach for generating GNSS orbit and clock products with centimeter-level accuracy, which is particularly important for BDS and the local commercial providers relying on a regional network. In the integrated Precise Orbit Determination (POD), LEO satellites are used to compensate for the drawback of regional ground stations in the precise orbit and clock determination of GNSS satellites. To validate the role of LEO satellites in the orbit determination with a regional network, 6 International GNSS Service stations around China and 13 LEO satellites from January 20 to 26, 2019, including GRACE-C/D, SWARM-A/B/C, Jason-3, Sentinel-3A/B, and SAT-A/B/C/D/E are selected in this study to perform the integrated POD. The orbit and clock accuracies of GPS and LEO satellites are evaluated by comparison with precise products. The average Root Mean Square (RMS)of GPS orbit errors in the radial (R), along-track (T) and cross-track (N) directions are 2.27 cm, 3.45 cm, and 3.08 cm, respectively, and the clock accuracy is better than 0.15 ns based on a comparison with the final products provided by Center for Orbit Determination in Europe (CODE). The LEO orbit accuracy is better than 2 cm in the R direction, and the position errors are mostly within 4 cm. The results indicate that the integrated POD can generate high-precision orbit and clock products for GPS and LEO satellites based on regional network stations. Finally, the integrated POD products are assessed for Precise Point Positioning (PPP). Simulated kinematic PPP has a comparable performance in terms of the convergence time and positioning accuracy. With more LEO satellites available, the orbit and clock determination accuracy and PPP positioning accuracy can be improved.

Keywords Global navigation satellite system, Precise orbit determination, Regional stations, Low earth orbit satellites, Orbit and clock accuracy

Introduction

GNSS plays an extremely important role in Positioning, Navigation, and Timing (PNT), and brings new opportunities for high-precision orbit determination of LEO satellites. With the successful launch of TOPEX/POSEIDON, the era of utilizing onboard GNSS data for LEO satellite orbit determination has officially begun (Tapley et al., 1994). In this POD approach, precise

*Correspondence:
Chengpan Tang
cptang@shao.ac.cn
[1] Shanghai Astronomical Observatory, Chinese Academy of Sciences, Shanghai 200030, China

orbit, and clock products of GNSS satellites are derived from ground station measurements. Subsequently, these precise products are utilized to conduct LEO POD by using onboard GNSS data. It is evident that the orbit determination accuracy for LEO satellites directly depends on the accuracy of GNSS satellite products. At present, the IGS Analysis Centers (ACs) utilize the data from many global ground stations to generate the real-time, ultra-rapid, rapid, and final products (https://igs.org/products/#about) for GPS, GLONASS, Galileo, and BDS. The POD accuracy of GNSS satellites is significantly influenced by the quantity and distribution of participating ground stations. Although well-distributed global ground stations are accessible to the scientific community, some commercial operators or BDS (Tang et al., 2018; Yang et al., 2020) choose to establish their own regional monitoring stations for the sake of system stability and reliability. Based on the regional network, it is impossible to generate GNSS satellite orbits and clock offsets with high accuracy, leading to the difficulty in providing high-precision services with GNSS.

In recent years, numerous LEO constellation projects have been rapidly developed, including Iridium (Fossa et al., 1998), StarLink (Khalife et al., 2021; Osoro & Oughton., 2021), OneWeb (Osoro & Oughton, 2021), and Boeing (Reid et al., 2016, 2018) in the USA, as well as CentiSpace (Yang, 2019) in China. These LEO constellations can provide communication services through Inter-Satellite Links (ISLs) while also offering PNT services by broadcasting ranging signals, message data and augmentation information to various users to meet the demands of precision, availability, integrity, and reliability (Yang et al., 2024). LEO satellites are typically equipped with onboard receivers and can function as mobile monitoring stations for achieving global tracking of GNSS satellites. This brings about new opportunities for enhancing GNSS satellite orbit determination accuracy by processing the observations from both LEO satellites and ground stations. Many studies have been performed using this approach, also named as "one-step" method (Zhu et al., 2004). This method has been adopted to improve the accuracy of the estimated orbits and Earth Orientation Parameters (EOP) (Geng et al., 2008; Huang et al., 2020; Hugentobler et al., 2005; König et al., 2005; Li et al., 2018; Zhao et al., 2017). Furthermore, the one-step method has also been proven effective in improving the stability of parameter estimations (Boomkamp & Dow, 2005), the rate of ambiguity fixing (Zoulida et al., 2016), and the accuracy of geocentric coordinates (Männel & Rothacher, 2017). Additionally, it can enhance data processing efficiency in various scientific and practical applications. However, in the existing studies, the accuracy of satellite clock offsets estimated with the one-step method has not been considered, and its performance in providing high-precision navigation services has also not been mentioned.

Given this background, we conduct the integrated POD processing experiments using the data from regional ground stations and LEO satellites. It is crucial to investigate the achievable accuracy of orbit and clock products with the integrated processing method. Furthermore, we need to analyze whether the products obtained with this approach can meet the demands of high-precision services. Although the monitoring station deployment of BDS is regional, it seems more meaningful to conduct integrated POD using BDS and LEO satellites. However, due to the data limitations, we currently cannot obtain redundant onboard BDS observation data from enough LEO satellites. Therefore, we take GPS satellites as an example, the integrated POD is conducted along with an accuracy assessment. The integrated POD strategy, which combines a regional network and 13 LEO satellites from January 20 to 26, 2019, is first introduced in Section "Strategy of integrated POD". Then, the accuracy of the derived GPS orbits, clock offsets and LEO orbits are assessed in section "Results and analysis". Besides, the GPS orbit and clock products are also validated with PPP using ground stations worldwide. A discussion and the conclusions are given in Section "Discussion and Conclusions".

Strategy of integrated POD

This section is divided into three parts. The first part briefly introduces the methodology of the integrated POD. The second part gives a detailed description of the experimental data used in this study, mainly the data from LEO satellites and ground stations. Finally, the models adopted and the parameter estimation strategy employed in the integrated POD are listed in detail.

Methodology

In the integrated POD, the Ionosphere-Free (IF) combinations of pseudo-range and phase observations of GNSS satellites tracked by ground stations and LEO satellites are used. The observation equations for a ground station and LEO satellite can be expressed as follows:

$$\begin{cases} P^s_{G,IF} = \rho^s_{G,IF} + \delta t_G - \delta t^s + T^s_G + b^s_{G,IF} - b^s_{IF} + \varepsilon^{s,p}_{G,IF} \\ P^s_{L,IF} = \rho^s_{L,IF} + \delta t_L - \delta t^s + b^s_{L,IF} - b^s_{IF} + \varepsilon^{s,p}_{L,IF} \\ L^s_{G,IF} = \rho^s_{G,IF} + \delta t_G - \delta t^s + T^s_G + \lambda_{IF} N^s_{G,IF} + B^s_{G,IF} - B^s_{IF} + \varepsilon^{s,l}_{G,IF} \\ L^s_{L,IF} = \rho^s_{L,IF} + \delta t_L - \delta t^s + \lambda_{IF} N^s_{L,IF} + B^s_{L,IF} - B^s_{IF} + \varepsilon^{s,l}_{L,IF} \end{cases} \tag{1}$$

where the subscript G represents ground stations, and L represents LEO satellites, the superscript S represents a specific GPS satellite. $P^s_{G,IF}$, $L^s_{G,IF}$, $P^s_{L,IF}$ and $L^s_{L,IF}$ are the pseudo-range and carrier phase observations received by

the ground station and LEO satellite. $\rho^s_{G,IF}$ and $\rho^s_{L,IF}$ represent the satellite-to-receiver distances for ground stations and LEO satellites relative to GNSS satellites. δt_G and δt_L denote the receiver clock offsets, respectively, whereas δt^s is the satellite clock offsets. T^s_G represents the tropospheric delay experienced by the ground station. $b^s_{G,IF}$ and $b^s_{L,IF}$ are the pseudo-range hardware biases for the receiver, whereas b^s_{IF} is for the satellite. $B^s_{G,IF}$ and $B^s_{L,IF}$ are the phase hardware biases for the receiver, whereas B^s_{IF} is for the satellite. λ_{IF} is the wavelength of IF combination. $N^s_{G,IF}$ and $N^s_{L,IF}$ are integer ambiguities for ground stations and LEO satellites. $\varepsilon^{s,p}_{G,IF}$, $\varepsilon^{s,p}_{L,IF}$, $\varepsilon^{s,l}_{G,IF}$ and $\varepsilon^{s,l}_{L,IF}$ represent the other corrections and error sources of pseudo-range and phase observations, such as tropospheric delays or multipath errors.

Then, based on the principle of statistical orbit determination, the observation model at time t_i can be expressed as follows (Montenbruck et al., 2002):

$$\begin{cases} Y_{STA,i} = G\left(X_{G,i}, X_{STA,i}, P_{G,i}, t_i\right) + \varepsilon_{STA,i} \\ Y_{L,i} = E\left(X_{G,i}, X_{L,i}, P_{G,i}, P_{L,i}, t_i\right) + \varepsilon_{L,i} \end{cases} \tag{2}$$

where $X_{G,i}$ and $X_{L,i}$ are the orbital parameters of GNSS and LEO satellites, respectively, and $X_{STA,i}$ represent the parameters related to the ground station, such as the station coordinates and tropospheric delay. $P_{G,i}$ and $P_{L,i}$ represent other parameters, such as clock offsets, ambiguities, solar radiation coefficients, atmospheric drag coefficients, and empirical parameters. $\varepsilon_{STA,i}$ and $\varepsilon_{L,i}$ represent the noise of ground station data and LEO onboard data, respectively.

According to the equation of motion and variational equations of GNSS and LEO satellites, their state transition matrices $\psi_G(t_i, t_0)$ and $\psi_L(t_i, t_0)$ can be obtained by numerical integration. They meet the following conditions:

$$\begin{cases} x_{G,i} = \psi_G(t_i, t_0) x_{G,0} \\ x_{L,i} = \psi_L(t_i, t_0) x_{L,0} \end{cases} \tag{3}$$

where $x_{G,i}$ and $x_{L,i}$ are the state vectors of GNSS and LEO satellites, respectively, $x_{G,0}$ and $x_{L,0}$ are the initial epoch states. Based on Eqs. (2) and (3), orbital and other parameters of the GNSS and LEO satellites can be solved by using the least squares estimation.

Experimental setup

For BDS or some commercial service providers who cannot control a global network, it is a good means to generate precise orbits by integrating the measurements from regional ground stations and LEO satellites. LEO satellites are equipped with onboard GNSS receivers, which can be regarded as a supplement to regional ground stations to achieve full-arc tracking of GNSS satellites. Therefore, in this section, we select 6 regional stations around China and the onboard data of 13 LEO satellites from January 20 to 26, 2019 to simulate the scenario of integrated POD.

LEO satellites

In recent years, an increasing number of LEO satellites have played important roles in the fields of gravity recovery, ocean altimetry, and atmospheric sounding. Considering the limitations of data access, the onboard GPS data of 13 LEO satellites are selected to conduct integrated POD processing. These LEO satellites are divided into five different missions. GRACE Follow-On is the continuation of GRACE's legacy tracking of Earth's water movement across the planet. Monitoring the changes in ice sheets and glaciers, underground water storage, the amount of water in large lakes and rivers, and the changes in sea level provides a unique view of Earth's climate and has far-reaching benefits for people (https://gracefo.jpl.nasa.gov/).

Swarm is the ESA's first mission for Earth Observation (EO). It consists of three identical satellites named Alpha, Bravo, and Charlie (A, B and C). Swarm is dedicated to creating a detailed survey of the Earth's geomagnetic field and its temporal evolution as well as the electric field in the atmosphere by using a satellite constellation that carries sophisticated magnetometers and other instruments (https://earth.esa.int/eogateway/missions/swarm).

The Jason-3 satellite is the follow-up altimetry mission of Jason-2/OSTM. Its objective is to provide the unique accuracy and coverage of the TOPEX/Poseidon, Jason-1, and OSTM/Jason-2 missions in support of operational applications related to extreme weather events, operational oceanography, and climate applications and forecasting.

Sentinel-3 is a multi-instrument mission that measures sea-surface topography, sea- and land-surface temperature, ocean color and land color with high accuracy and reliability. The mission supports ocean forecasting systems, as well as environmental and climate monitoring (https://www.esa.int/Applications/Observing_the_Earth/Copernicus/The_Sentinel_missions).

SAT-A/B/C/D/E are Chinese satellites using GNSS Radio Occultation (GNSS-RO) to collect atmospheric data for weather prediction and for ionosphere, climate, and gravity research. These satellites are capable of profiling vertical parameters such as temperature, humidity, and pressure in the middle and lower latitudes globally. It provides high vertical resolution and accurate observations for numerical weather prediction. The detailed information is shown as follows (Table 1).

Table 1 Detailed information on the 13 selected LEO satellites

Satellite	Abbreviation	Altitude/km	Inclination/deg
GRACE-C	GRCC	483	89
GRACE-D	GRCD	483	89
SWARM-A	SWMA	450	87.4
SWARM-B	SWMB	530	88
SWARM-C	SWMC	450	87.4
JASON-3	JAS3	1336	66
SENTINEL-3A	SN3A	814.5	98.65
SENTINEL-3B	SN3B	814.5	98.65
SAT-A	SATA	802	50
SAT-B	SATB	802	50
SAT-C	SATC	802	50
SAT-D	SATD	802	50
SAT-E	SATE	802	50

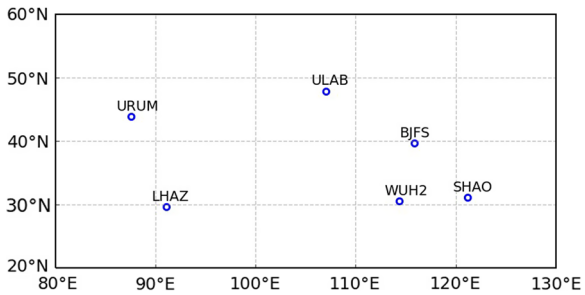

Fig. 1 Distribution of 6 IGS ground stations

Regional ground stations

Some providers, including BDS and other commercial companies, are unable to autonomously control and maintain well-distributed global ground stations. Regional stations are more likely to be available. In this study, 6 IGS stations (Johnston et al., 2017) around China, namely, SHAO, BJFS, WUH2, URUM, LHAZ, and ULAB, are selected to simulate regional network tracking. Their distribution is shown in Fig. 1.

POD strategy

We use the software platform called ShangHai ORbit DEtermination (SHORDE) (He et al., 1988), which was developed by Shanghai Astronomical Observatory (SHAO), Chinese Academy of Sciences (CAS), to perform the integrated POD. SHORDE is capable of processing the data from various sources such as GNSS, Satellite Laser Ranging (SLR), Doppler Orbitography and Radio Positioning Intergrated by Satellite (DORIS), and ISLs to estimate the orbit and clock offsets of GNSS and LEO satellites, as well as performing PPP solution and other geodetic applications. For the configuration of POD strategy, the arc length is 24 h, the data sampling interval is 30 s, and the elevation cutoff is 5°. L1 and L2 dual-frequency IF combinations of pseudo-range and phase observations are used in the data processing. The detailed strategy is given in Tables 2 and 3. To correct for antenna Phase Center Offsets (PCOs) and Variations (PCVs), we utilize the absolute phase centers (Schmid et al., 2007) to obtain the corrections for GPS satellites and ground stations. PCOs are applied for LEO onboard receivers, while PCVs are disregarded in this study. PCOs of GRCC and GRCD are obtained from the products (VGN1B) published by JPL. SWMA, SWMB, and SWMC utilize the satellite-specific ionosphere-free combined PCOs offered by the European Space Agency (ESA) (Siemes, 2019). For JAS3, the PCOs are obtained from the prior values provided by Centre National d'Etudes Spatiales (CNES) (Couderc, 2015). SN3A and SN3B use the ground-calibrated reference point and PCOs (Fernández Martìn, 2016), and SATA, SATB, SATC, SATD and SATE use the prior values provided by satellite operators. Regarding the satellite attitude, the measured quaternion data provided by operators are used for GRCC, GRCD, SWMA,

Table 2 The models adopted in the integrated POD

Dynamic Models	GPS	LEO
Atmospheric Drag	Not applied	Box-wing model; DTM94 density model is used for calculation of atmospheric density
Earth gravity field	EGM2008(12 × 12)	EGM2008(140 × 140)
Solar radiation pressure	5-parameter model (Arnold et al., 2015)	Box-wing model
Earth radiation pressure	(Rodriguez-Solano et al., 2012)	Not applied
N-body perturbation	JPL DE430 (Folkner et al., 2014)	JPL DE430
Relativity	IERS Conventions 2010 (Petit & Luzum, 2010)	IERS Conventions 2010
Solid earth, pole tide	IERS Conventions 2010	IERS Conventions 2010
Ocean tide	FES2004	FES2004

Table 3 The parameter estimation strategy in the integrated POD

Observation models	Descriptions
Data source	GRACE-C/D: GFZ Potsdam Information System and Data Center (ISDC) SWARM-A/B/C: ESA JASON-3: Archivage Validation et Interprétation des données des Satellites Océanographiques (AVISO) Sentinel-3A/B: ESA SAT-A/B/C/D/E: satellite operators
Arc length	24 h
Cutoff elevation	5°
GPS antenna PCO/PCV	igs14_2035.atx
LEO antenna PCO/PCV	PCOs are offered by satellite operators, and PCVs are not applied
LEO attitude	Quaternions provided by satellite operators for the former 8 LEO satellites, and nominal attitude for SAT-A/B/C/D/E
Observation type	Undifferenced IF combinations of carrier phase and pseudo-range measurements
Weight	Ground and LEO observations are equally weighted
Sampling rate	30 s for both ground and onboard observations
Station coordinates	Fixed to IGS weekly solutions
Estimated parameters	
Station coordinates	Tightly constrained
GPS orbit	6 orbital elements calculated with broadcast ephemeris; 5 ECOM solar radiation pressure parameters: 24 h
LEO orbit	6 orbital elements based on the single-point positioning (SPP); piecewise empirical parameters: 3 h drag scale coefficient: 1.5 h solar radiation pressure coefficient: 3 h for JAS3, 12 h for others
Tropospheric delay	For each ground station; piecewise constant zenith delays for 1 h intervals; piecewise constant horizontal gradients for 4 h intervals
Phase ambiguities	Float
Clock offsets	Satellites and receivers; epoch wise; pre-eliminated
Earth rotation parameters	Fixed as known values with a priori value: IERS Bulletin A product; Rotation pole coordinates and UT1 for 24 h intervals; piece-wise linear modeling

SWMB, SWMC, JAS3, SN3A and SN3B. Meanwhile, the remaining 5 LEO satellites adopt the geocentric stabilization attitude mode. To ensure data quality, the Turboedit algorithm (Blewitt, 1990) is employed for cycle slip detection. A weight ratio of 1:10,000 is set for pseudo-range to phase observations. Additionally, a threshold of three times the mean square error is utilized to edit the residuals of orbit determination.

Both GPS and LEO satellites experience perturbation forces, including conservative and nonconservative forces. As for conservative forces, the Earth's gravitational force is modeled using EGM2008 (Pavlis et al., 2012). Considering the magnitude of perturbations, low-order gravitational models are employed for GPS satellites, while high-order gravitational models are used for LEO satellites. IERS Conventions 2010 is adopted to describe solid tide and pole tide, as well as for the computation of relativity effects. FES 2004 (Lyard et al., 2006) model is used to account for ocean tides. However, accurate modeling of nonconservative forces such as atmospheric drag and solar radiation pressure remains challenging due to various factors like atmospheric density variations, solar activity, and spacecraft characteristics. To compensate for the model errors associated with nonconservative forces, it is necessary to estimate additional force model parameters, such as the solar radiation coefficient, drag scale coefficient, and empirical parameters. For the computation of solar radiation pressure, we utilize the 5-parameter ECOM model for GPS satellites and the box-wing model for LEO satellites. Atmospheric drag is modeled using the box-wing model, which considers the atmospheric density computed with DTM94 (Berger et al., 1998) for LEO satellites. In addition, a drag scale coefficient is estimated every 1.5 h to represent the variability of atmospheric drag more accurately. The perturbation of atmospheric drag on GPS satellites is negligible. Ambiguities are solved but not fixed to integers. The satellite clock parameters are treated as white noise,

and a set of satellite clock offsets and receiver clock offsets are estimated per epoch. The detailed strategy can be found in Tables 2 and 3.

Results and analysis

Visibility analysis

For the integrated POD, both LEO satellites and ground stations track the signals from GPS satellites. The number of GPS satellites tracked by a LEO satellite will affect the accuracy of determined LEO satellite orbits. The number of receivers tracking GPS satellites, regardless of the LEO on-board receivers or the ground station receivers, will affect the orbit accuracy of GPS satellites. Therefore, whether it is for GPS or LEO satellites, conducting satellite visibility analysis is essential to obtain high-precision orbit and clock products.

Number of GPS satellites tracked by a LEO onboard receiver

When using the onboard GPS data to perform LEO POD, a larger number of visible GPS satellites provides more redundant observations, ensuring greater stability in parameter estimation. We take the selected 13 LEO satellites from 00:00 to 24:00 on January 20, 2019 as an example, a comprehensive analysis of the minimum, maximum, average, and valid numbers of tracked GPS satellites is illustrated in Fig. 2. The satellites with dual-frequency observations are considered valid.

From Fig. 2, the number of GPS satellites tracked is very similar for the same LEO satellite mission, mainly due to two reasons: (1) Satellites of the same LEO mission carry the same type of onboard receivers and have the same number of satellite tracking channels; (2) Satellites of the same mission also have similar orbital heights, inclinations, and orbital types. Therefore, for the same LEO satellite mission, the number of GPS satellites tracked by each individual LEO satellite within the mission is similar. From the satellite visibility results on January 20, 2019, a minimum of 5 satellites and a maximum of 10 satellites are tracked by GRCC and GRCD. On average, they track 8.7 and 8.9 GPS satellites, respectively, and the data efficiency reaches 100%. For SWMA, SWMB and SWMC, the number of tracked GPS satellites ranges from 6 to 8, with an average of 7.9 and the data efficiency of 97.5%. For JAS3 which circles in a near-polar orbit, the number of tracked satellites varies with the maximum of 12, the minimum of 2, the average of 9.7, and the data efficiency of 97.9%. For SN3A and SN3B, the number of tracked satellites ranges from 5 to 8 with an average of 7.7, and the data efficiency of 97.9%. For the remaining 5 satellites of SATA, SATB, SATC, SATD and SATE, the maximum number is 12, the minimum number is not less than 5, the average number is above 10, and the data efficiency of SATC is the lowest and reaches 91.8%. The maximum and average number of GPS satellites tracked of SATA, SATB, SATC, SATD, and SATE are equivalent to that of JAS3, but the data efficiency is slightly lower than that of JAS3. The average number of GPS satellites tracked by SWMA, SWMB, and SWMC are slightly larger than that of JAS3, but the data efficiency is almost the same.

The selected 13 LEO satellites are all equipped with on-board receivers, which can track 8 to 10 GPS satellites on average. Therefore, the onboard observations can serve as an important data source in the GPS satellites orbit determination, especially under the conditions of regional network deployment.

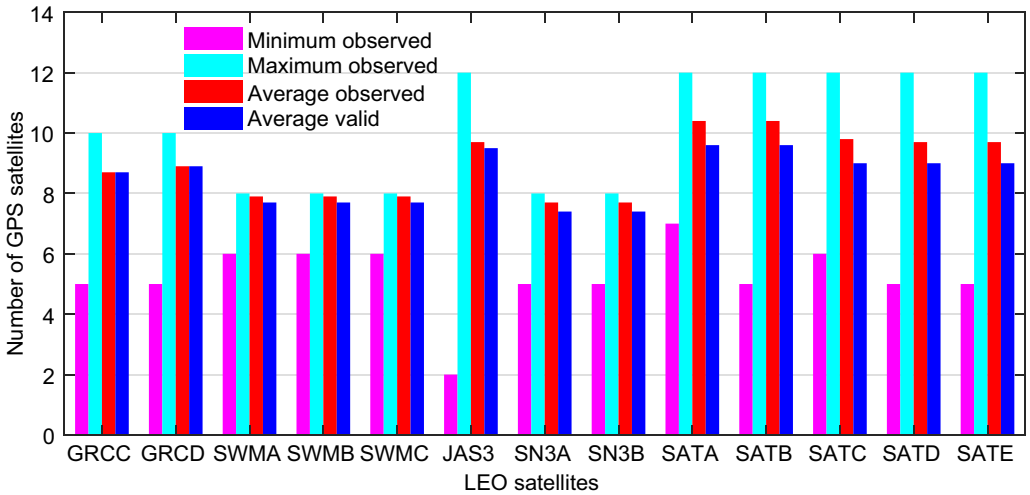

Fig. 2 Number of GPS satellites tracked by 13 LEO satellites

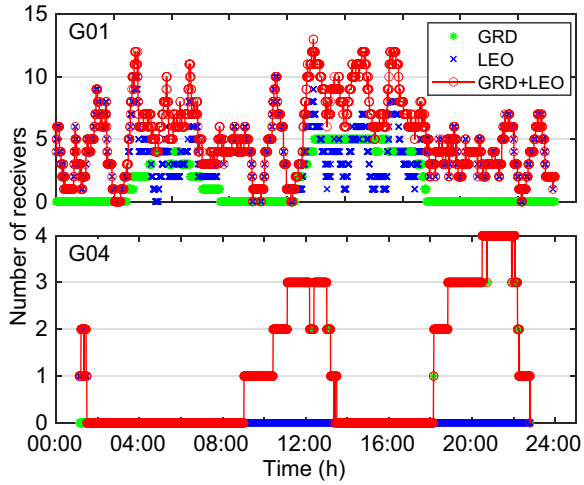

Fig. 3 Number of receivers tracking G01 and G04 from 00:00 to 24:00 on January 20, 2019

Number of Receivers tracking GPS satellites

The number of receivers tracking GPS satellites directly affects the orbit and clock determination accuracy of GPS satellites. Figure 3 takes G01 and G04 as an example to analyze the number of receivers on January 20, 2019. In Fig. 3, the ground stations denoted by a green star is abbreviated as "GRD", the LEO satellite denoted by a blue cross is abbreviated as "LEO", and the combination of ground station and LEO satellite denoted by a red line-circle is abbreviated as "GRD + LEO".

Figure 3 illustrates that the 6 regional ground stations exhibit brief tracking arcs for G01 and G04 with prolonged periods during which the number of ground receivers drops to zero. Consequently, relying solely on regional ground receivers makes it impossible to estimate high-precision orbits for GPS satellites. After involving 13 LEO satellites, the receivers tracking satellite G04 are scarce for both ground stations and LEO satellites. Therefore, subsequent accuracy assessments will not consider satellite G04. Meanwhile, for satellite G01, the maximum number of tracking receivers rises from 5 to 13, and the proportion of receivers being zero has significantly decreased from 55% to 2%. It indicates that the issue of tracking gaps resulting from the limited coverage of 6 regional ground stations can be effectively resolved with the inclusion of LEO satellites. Typically, there is at least one receiver tracking G01 most time on January 20, 2019. However, there are still some epochs at which no receivers can track G01. The lack of continuous tracking may result in the initialization of all ambiguity parameters in the orbit determination process. Figure 4 gives the average number of receivers tracking the GPS satellites.

According to Fig. 4, the average number of receivers for satellite G04 remains unchanged before and after the inclusion of LEO satellites. This consistency arises due to the limited capability of the selected 13 LEO satellites to receive observations from satellite G04. Conversely, for the remaining 31 satellites, the average number surges from 2.3 to 5.9, marking a substantial increase of 61.4%. This underscores the notable enhancement in receiver visibility to GPS satellites facilitated by the integration of LEO satellites, consequently benefiting the orbit determination process for GPS satellites.

Accuracy of determined orbit and clock

When the integrated POD is completed, the final products released by CODE are selected as a reference to

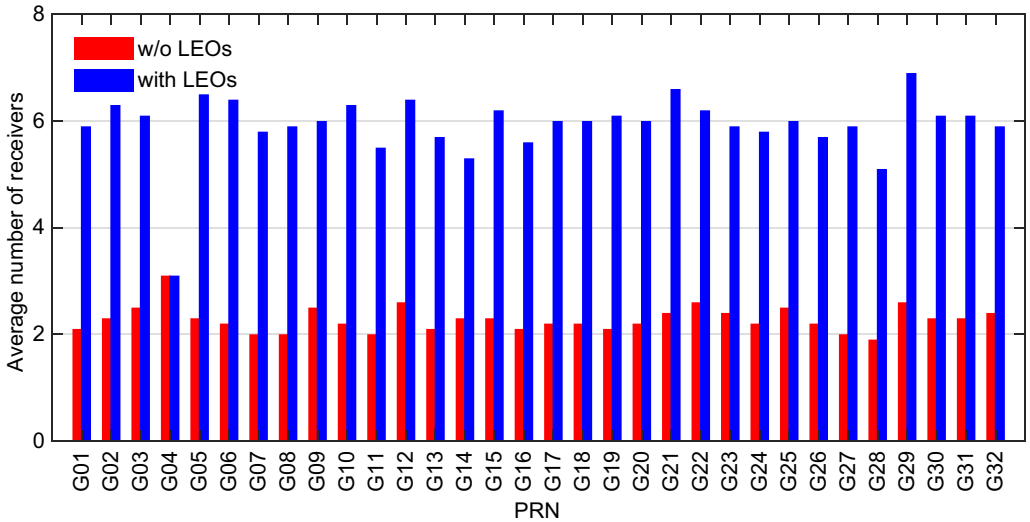

Fig. 4 The average number of receivers tracking GPS satellites

evaluate the orbit and clock accuracy of the GPS satellites. For LEO satellites, the corresponding organizations of the former 8 satellites have released Post Science Orbits (PSOs). Therefore, we can compare the LEO orbit derived from the integrated POD with PSOs to evaluate the orbit accuracy. However, for SAT-A/B/C/D/E, due to the absence of official precise orbit products, this study evaluates the orbit accuracy of these 5 LEO satellites using two approaches. The first one is comparing overlapping orbits and the second one compares the orbits derived from the integrated POD with the orbits solved by introducing fixed COD final GPS orbit and clock products provided to IGS. To avoid the errors resulting from different spatial datum used, this study considered the Helmert 7-parameter transformation when conducting orbit accuracy assessments.

GPS satellite orbit accuracy

To evaluate the role of LEO satellites in GPS satellite orbit determination, we first conducted orbit determination based on the measurements from the regional network only. The primary distinction in the POD strategy for the regional network compared to Tables 2 and 3 is that the arc length is set to 72 h. Figure 5 shows the orbit comparisons in the R, T, N and 3-dimensional (3D) direction between the COD orbits and those of the other 31 GPS satellites excluding G04, calculated by the regional network POD from January 20 to 26, 2019. The average RMS value in the R, T, N, and 3D direction is 0.32 m, 1.07 m, 0.52 m, and 1.23 m, and orbit accuracy is relatively stable from day to day, indicating the appropriate orbit determination strategy and reliable observation data. Based on this, it clearly indicates that with the regional network POD, only meter-level precision orbit products can be obtained, which is obviously insufficient to meet the demand for high-precision navigation services.

Figure 6 shows the orbit comparisons in the R, T, N and 3D direction between the COD orbits and those orbits of the other 31 GPS satellites excluding G04 calculated by the integrated POD on January 20, 2019. The horizontal axis represents the PRN of GPS satellites, and the vertical axis represents the RMS of the orbit differences for each satellite.

From Fig. 6, the derived GPS satellite orbits achieve centimeter-level accuracy compared to the COD final products. Among the three components, the R direction exhibits the smallest RMS, averaging 2.32 cm. It's followed by the T direction with an average of 3.65 cm and the N direction with an average of 3.14 cm. The average RMS of 31 GPS satellites excluding G04 during January 20–26, 2019, are shown in Fig. 7.

In Fig. 7, we performed the integrated POD for 7 days, the average RMS in the R, T, and N direction is 2.27 cm, 3.45 cm, 3.08 cm, and the average RMS in the 3D direction is 5.15 cm. Compared with the orbits based on the regional network only in Fig. 5, the orbit accuracy in R, T, N, and 3D direction has been improved by 92.9%, 96.8%, 94.0%, and 95.8% respectively. The results demonstrate that the involution of LEO satellites can effectively compensate for the deficiency of insufficient tracking arcs, and the orbit errors are greatly reduced, which agree to the existing findings in Konig et al. (2005), Hugentobler et al. (2005), Geng et al. (2008), Zhao et al. (2017), Li et al. (2018), Huang et al. (2020).

Li et al. (2022a) conducted GNSS orbit determination by processing more than 150 globally distributed Multi-GNSS Experiment (MGEX) stations. Among them, GPS orbits have the highest accuracy, with an average 3D

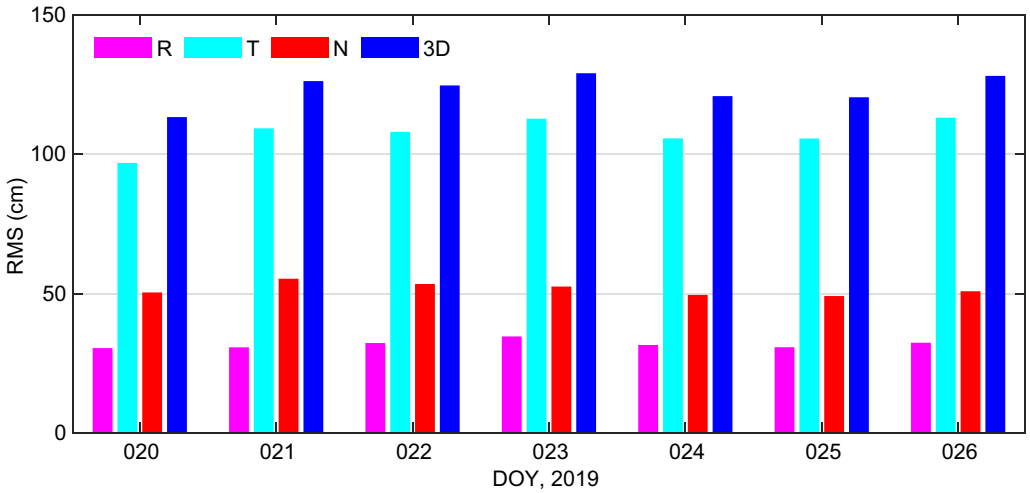

Fig. 5 Orbit comparisons between regional network POD and COD final products during DOY 20–26, 2019

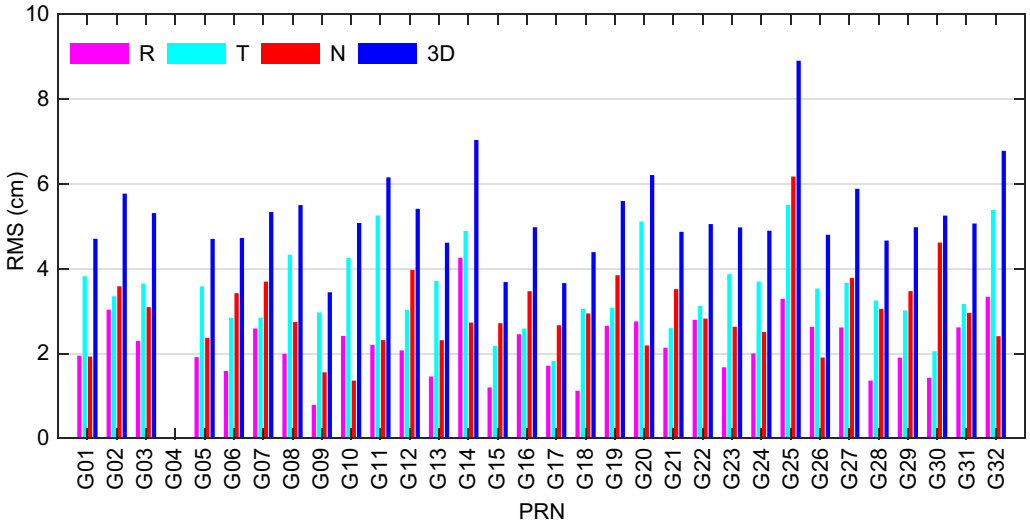

Fig. 6 Orbit comparisons between the integrated POD and COD final products during DOY 20–26, 2019

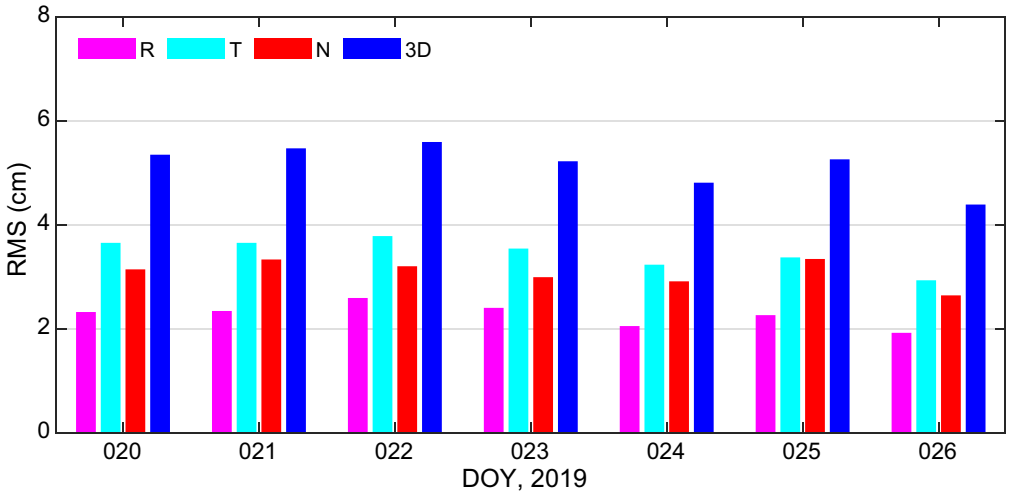

Fig. 7 Orbit comparisons between the integrated POD and COD final products during DOY 20–26, 2019

RMS of 2.11 cm. Obviously, the integrated GPS orbit accuracy is slightly worse than the orbit accuracy generated with a large global network from Li et al. (2022a), which can be attributed to that the regional network and insensitivity of the inter-satellite link measurements to the orbit orientation angles account for the larger normal orbit error of GPS satellites. The measurements from LEO onboard receivers are in fact some kind of satellite-to-satellite ranging measurements, which are insensitive to any motion of the constellation as a rigid body and the orientation parameters including inclination and the right ascension of ascending node. Therefore, adding the LEO satellites does not give constraints in the normal direction as strong as in the radial and cross-track directions. The error in the normal direction for GPS orbits of the integrated POD products is larger than the IGS products due to the regional stations used. In addition, the problem of insufficient observations still exists, though 13 LEO satellites are involved, because there are some epochs when no receivers track GPS satellites. Moreover, the ambiguities solved in this contribution are float solution. All these factors affect the accuracy of GPS orbit determination. However, the accuracy is indeed at the same level, approximately within a few centimeters.

LEO orbit accuracy

Since there is no official organization to release precise orbits for SAT-A/B/C/D/E, we first evaluate the orbit

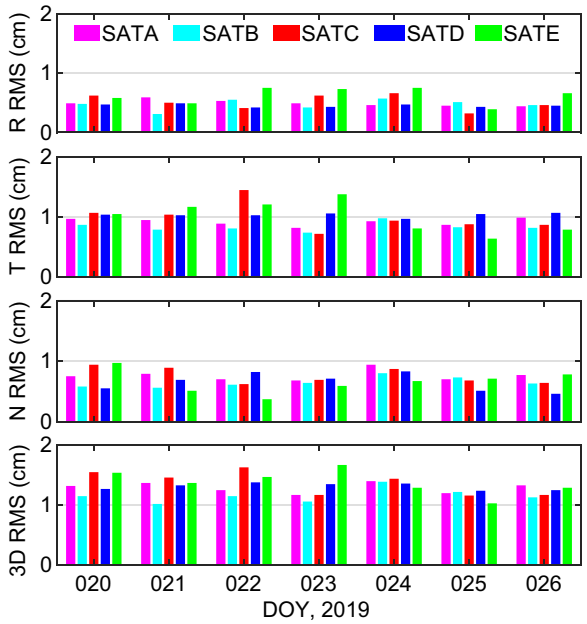

Fig. 8 RMS values in the R, T, N, and 3D direction of overlapping orbits derived from the integrated POD during DOY 20–26, 2019

Table 4 Average RMS of overlapping orbits for SAT-A/B/C/D/E derived from the integrated POD during DOY 20–26, 2019 (unit: cm)

LEO	R	T	N	3D
SATA	0.49	0.92	0.76	1.29
SATB	0.47	0.83	0.65	1.16
SATC	0.51	1.00	0.76	1.37
SATD	0.45	1.04	0.65	1.31
SATE	0.62	1.01	0.66	1.38

accuracy by comparing overlapping arcs. Assuming the current time is day0, the first orbit arc is set from 00:00 to 24:00 on day0, and the second orbit arc is shifted forward by 12 h, i.e., from 12:00 on day0 to 12:00 on day1, resulting in a 12-h overlapping orbits between the two arcs. To avoid the boundary effects, 1-h of orbit data is removed from each end of the 12-h overlapping arc, focusing on the 10-h overlapping orbit. Figure 8 shows the RMS values of overlapping arc differences in the R, T, N, and 3D direction. The horizontal axis represents the DOY in 2019, and the vertical axis represents the RMS of the overlapping orbit differences for each satellite. Table 4 shows the average RMS of the 5 LEO satellites. The accuracy of the overlapping arcs in the R direction is better than 1 cm and better than 2 cm in the 3D direction.

After a thorough comparative analysis of overlapping arcs, the orbit accuracy of SAT-A/B/C/D/E can achieve an internal consistency accuracy of better than 2 cm. Figure 9 shows the orbit comparisons in the R, T, N and 3D direction between the reference orbits and the orbits derived from the integrated POD of 13 LEO satellites on January 20, 2019. To establish the reference orbit, we utilized a zero-difference orbit determination algorithm, introducing the fixed GPS satellite precise orbit and clock products provided by CODE to compute the orbits of SAT-A/B/C/D/E satellites. Following that, we chosen this orbit as the reference for accuracy assessment. The horizontal axis represents the abbreviations of the LEO satellites, and the vertical axis represents the RMS of the orbital difference for each satellite.

As shown in Fig. 9, when orbit determination is conducted for 13 LEO satellites on January 20, 2019, the R direction has the smallest RMS value, better than 2 cm, while the RMS in the T direction is maximal. The RMS in the 3D direction is better than 4 cm compared to the reference orbit. Figure 10 gives the detailed statistical results over 7 days. The horizontal axis represents the DOY from 20 to 26 in 2019, and the vertical axis represents the RMS values in the R, T, N, and 3D direction for each day. Table 5 shows the average RMS of 13 LEO satellites derived from the integrated POD.

From Fig. 10 and Table 5, the RMS values for a period of 7 days are better than 2 cm and 5 cm in the R and 3D direction. The orbit accuracy in the T direction is the worst, primarily due to the influence of atmospheric drag perturbation, which is challenging to be accurately modeled. LEO POD is usually done by fixing precise orbit and clock products of GNSS satellites generated with the measurements from global stations as known values. The results indicate that with the integrated POD it is possible to generate precise LEO orbits with centimeter-level in a regional network.

Kang et al. (2020), van den Ijssel et al. (2015), Duan & Hugentobuler (2021) and Li et al., (2022b) reported that 1-3 cm orbit determination accuracy of LEO satellites is achievable by fixing the IGS GNSS satellite orbits generated with well-distributed global stations. Compared with the above results, the orbit accuracy of LEO satellites calculated by the integrated POD is slightly worse. The small number of regional receivers involved in the integrated orbit determination accounts for the larger orbit errors. Also, the refined processing strategy can help improve the LEO orbit determination, such as ambiguity resolution (Duan & Hugentobuler, 2021; Jiang et al., 2023; Zhang et al., 2021), which will be done soon.

c) GPS satellite clock accuracy.

In the process of the integrated POD, the orbital parameters and clock offsets of the GPS satellites are estimated simultaneously. To evaluate the accuracy of clock offsets, 2-order difference method is introduced between

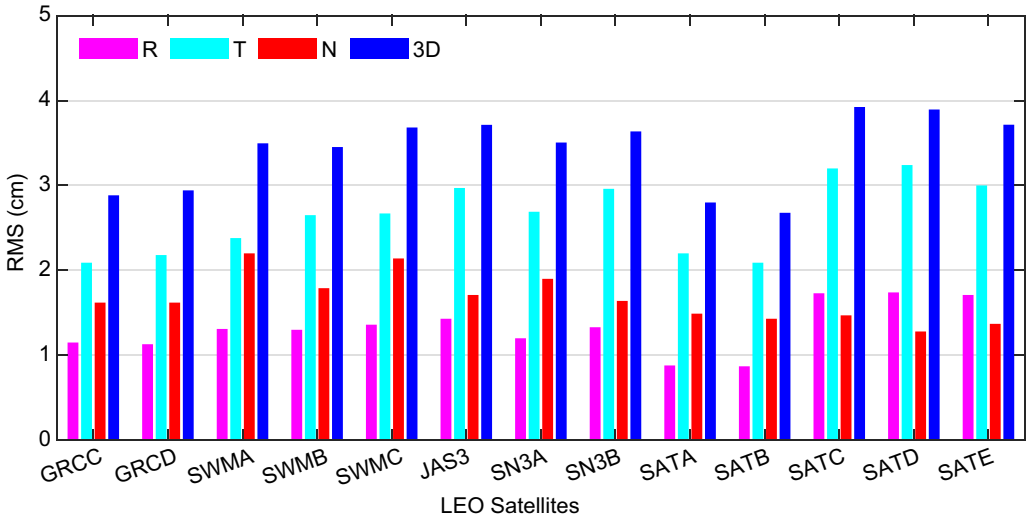

Fig. 9 Orbit comparisons of 13 LEO satellites between the integrated POD products and COD final products on January 20, 2019

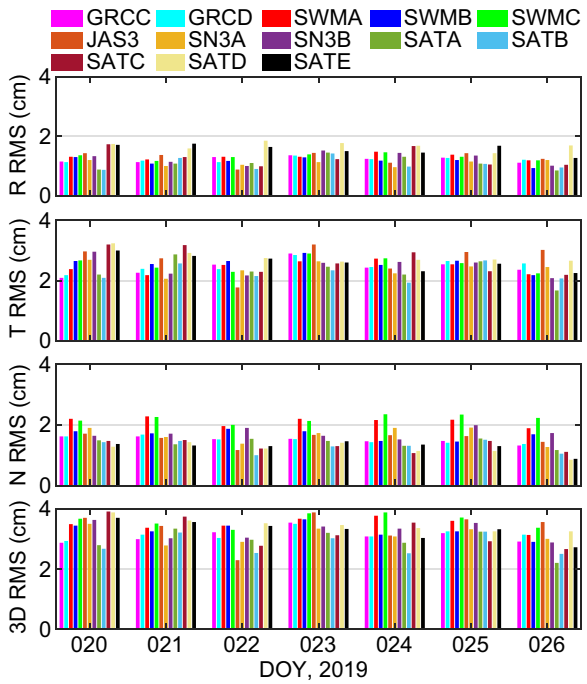

Fig. 10 Orbit comparisons of 13 LEO satellites between the integrated POD products and COD final products during DOY 20–26, 2019

Table 5 Average RMS of 13 LEO satellites derived from the integrated POD during DOY 20–26, 2019 (unit: cm)

LEO	R	T	N	3D
GRCC	1.22	2.44	1.51	3.12
GRCD	1.21	2.50	1.51	3.16
SWMA	1.31	2.46	2.12	3.51
SWMB	1.16	2.59	1.68	3.31
SWMC	1.31	2.55	2.21	3.62
JAS3	1.27	2.72	1.55	3.38
SN3A	1.10	2.41	1.67	3.14
SN3B	1.26	2.46	1.73	3.27
SATA	1.11	2.33	1.41	2.95
SATB	1.07	2.26	1.29	2.82
SATC	1.29	2.67	1.31	3.25
SATD	1.68	2.80	1.21	3.49
SATE	1.57	2.61	1.28	3.31

the results calculated by the integrated POD and COD final precise clock products, and the Standard Deviation (STD) of the 2-order differences is given as the final accuracy evaluation. The evaluation steps are expressed as:

(1) Select one GPS satellite as reference, and the clock offsets of other satellites are compared with the reference satellite to obtain 1-order differences at time t_i.

$$\Delta_{pod,i} = \delta t^{s}_{pod,i} - \delta t^{ref}_{pod,i} \tag{4}$$

$$\Delta_{cod,i} = \delta t^{s}_{cod,i} - \delta t^{ref}_{cod,i} \tag{5}$$

(2) Calculate the difference of the 1-order difference series, so that the influence of the reference difference can be eliminated, and the 2-order differences of the clock offsets can be obtained,

$$\Delta\nabla_i = \Delta_{pod,i} - \Delta_{cod,i} \tag{6}$$

(3) Compute the STD value of the 2-order differences.

$$STD = \sqrt{\frac{\sum_{i=1}^{n} \left(\Delta\nabla_i - \overline{\Delta\nabla}\right)}{n-1}} \tag{7}$$

where the subscript *pod* and *cod* denote the integrated POD products and COD final products, respectively. The subscript i indicates the sampling epoch. Δ and $\Delta\nabla$ means to make 1- and 2-order difference. The subscript n represents the total number of epochs. $\overline{\Delta\nabla}$ is the mean value of the 2-order differences.

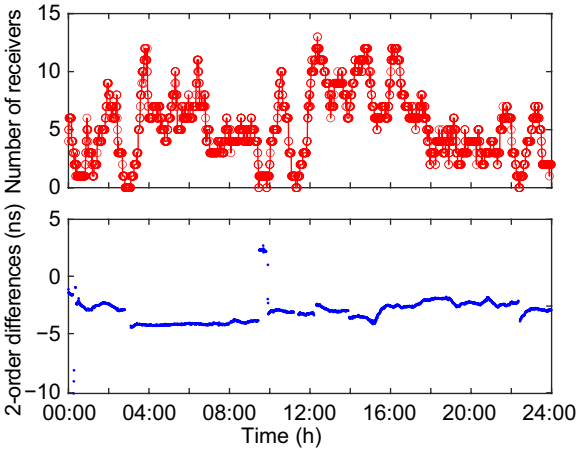

Fig. 11 The relationship between 2-order differences and the number of receivers

Continuous tracking of GPS satellites is crucial for ensuring the accuracy of satellite clock offsets. In visibility analysis for a specific GPS satellite there are the epochs when the number of receivers is zero. In this case, the clock offsets cannot be solved. When the satellite is tracked again, the 2-order difference of the clock offsets at this epoch will experience a certain degree of jump. This is mainly because for the estimation of clock offsets a reference datum needs to be selected first. When data gaps occur in GPS tracking, it will lead to a switch in the selected reference, resulting in discontinuity in the estimated clock offsets. In this case, G10 is chosen as the reference datum for computing the 2-order differences in clock offsets. Figure 11 takes G01 as an example, the time series of 2-order differences between G01 and G10 is presented.

From Fig. 11, the 2-order difference series exhibit a certain degree of jump when the number of receivers is zero. This indicates a switch in the reference datum for clock offsets. Therefore, when evaluating the accuracy of clock offsets, it is necessary to perform segmented statistical analysis on the 2-order difference sequence. Figure 12 shows the RMS and STD values of the segmented 2-order differences between the clock offsets calculated by the integrated POD and the COD clock products.

Due to the limited observations of G04, G10 has been selected as the reference datum. Consequently, these two satellites are excluded from the statistical analysis. From Fig. 12, it is evident that among the remaining 30 satellites, although systematic biases exist between the clock offsets derived from the integrated POD and the COD final precise clock products, these biases can be entirely absorbed by the receiver clock offsets in the positioning model without affecting the positioning accuracy (Ye,

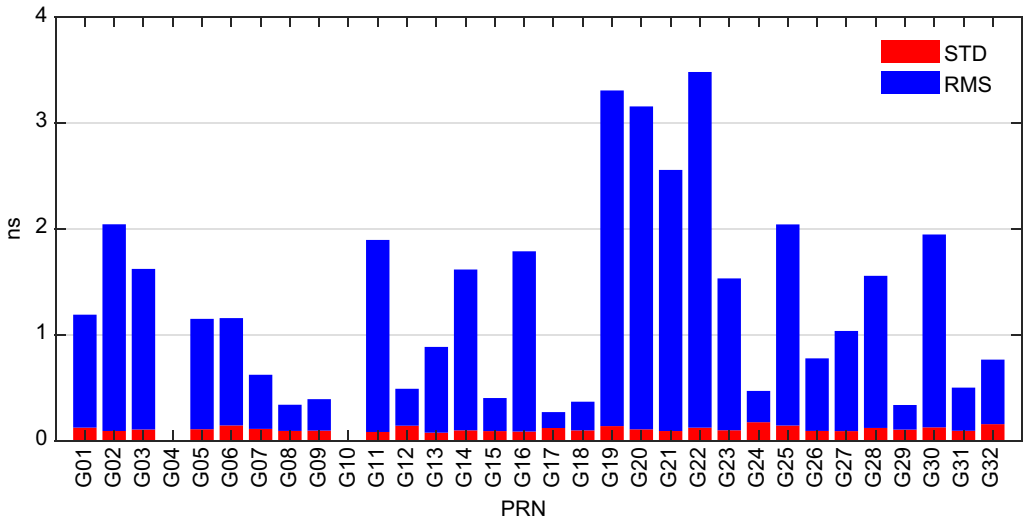

Fig. 12 The RMS and STD of 2-order clock differences of integrated POD compared with the COD final precise clock offsets

2002). Most of the STD values are better than 0.15 ns. Thus, with the integrated processing of the measurements from LEO satellites and regional ground stations, GPS satellite clock offsets with centimeter-level precision can be achieved.

PPP validation

After evaluating the accuracy of orbit and clock products, it is necessary to carry out positioning experiment using the products derived from the integrated POD. We selected the observation data of 18 IGS stations and conducted simulated kinematic PPP scenarios and discussed the impact of the discontinues in clock parameters estimation of GPS satellites. The PPP strategy is shown in Table 6. Although the stations are static, the station coordinates are treated as white noise and estimated epoch wise to assess the performance of the integrated POD products. The performance is assessed in terms of the convergence time and positioning accuracy. For comparison, simulated kinematic PPP validation is also carried out using the COD precise final products. The distribution of selected stations used for PPP validation is shown in the figure below (Fig. 13).

Convergence time

PPP is a convergence process that requires a long period of data accumulation to obtain an ideal positioning result. The convergence condition requires that the horizontal absolute positioning error remain below 10 cm and the vertical remain below 20 cm for at least 5 min in the corresponding direction. The average convergence time for the 18 IGS stations is given in Fig. 14.

For the stations CHUR, CRO1, HOB2, and WHIT, the convergence time is significantly shorter when using POD products compared to using COD products. However, for most stations, the convergence time using POD products is longer than or equal to the convergence time using COD products.

Positioning accuracy

To verify the effects of the integrated POD products on kinematic PPP positioning accuracy, we compare the positioning results with the precise coordinates provided in the SINEX file released by IGS analysis center and give the differences in the north (N), east (E) and up (U) directions. The kinematic PPP with the COD final products is also calculated for comparison purpose. The station-specific positioning accuracy is given in Fig. 15. The average accuracy is summarized in Table 7.

In Fig. 15, the feasibility of the integrated products for PPP applications is verified and decimeter-level positioning accuracy can be obtained. From Table 7, positioning accuracy with the COD products are slightly better than those with the POD products but at the same level. It can be attributed to the larger orbit errors and clock offset errors of the integrated POD products compared to the COD products. Based on the visibility analysis, the GPS satellites are not always tracked by two or more receivers. There are the epochs when some GPS satellites are not tracked by any

Table 6 PPP strategy adopted in this research

	PPP Strategy
Observation type	Undifferenced IF combinations of pseudo range and carrier phase observations from 18 IGS stations
Frequency band	L1/L2 IF combinations for GPS
Cutoff elevation	10°
Sampling rate	30 s
GPS orbits and clock offsets	The integrated POD products and COD final products
Observation weight	Code: phase = 1:10,000
GPS satellites and receivers' antenna PCO/PCV	igs14_2194.atx
Station displacement	Solid Earth tide, pole tide, ocean tide loading corrected (Petit & Luzum, 2010)
Relativistic	Corrected (Kouba, 2004)
Troposphere delay	Saastamoinen model (Saastamoinen, 1972) for wet and dry hydrostatic delay with the VMF1 (Boehm et al., 2006); residual tropospheric delay as a random-walk process
Ionosphere delay	The first-order ionosphere delay is eliminated by the dual-frequency combinations
Receiver clock	One receiver clock offset is set and estimated as white noise. The initial value is given as 0 and prior covariance is given as $9*10^{12}$ m^2
Receiver position	Estimated as white noise
Phase ambiguities	Estimated as float solutions and are not fixed as integers
Estimation	Forward Kalman filter

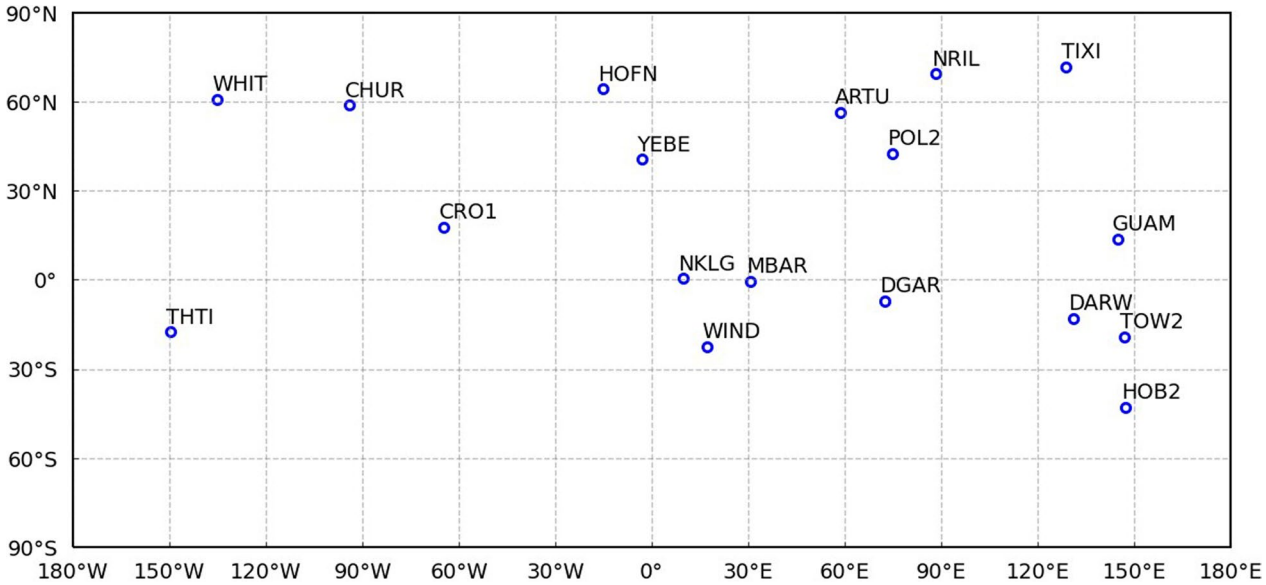

Fig. 13 Distribution of 18 IGS stations used for PPP validation

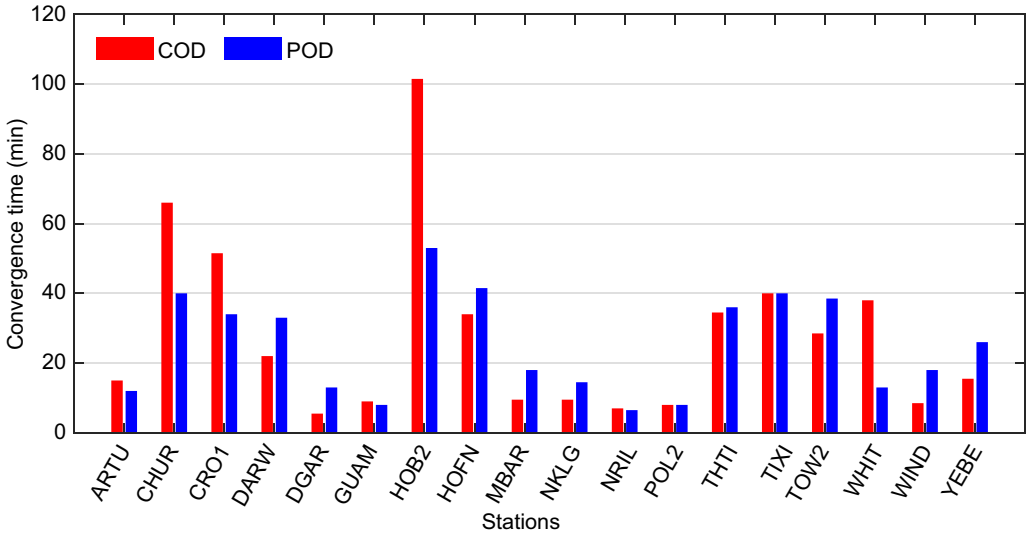

Fig. 14 The convergence time of kinematic PPP based on COD final products and integrated POD products

receivers, resulting in unattainable clock offsets for the GPS satellites and the discontinues in clock parameters estimation. In the PPP processing with the integrated POD products, the number of available satellites is smaller than the number with COD products at a few epochs, the ambiguity parameters should be reset and estimated, resulting in larger positioning errors. With more LEO satellites participating in the integrated orbit determination, it is believed that the data gap of GPS satellite tracking will no longer exist. The estimated clock offsets will also become continuous, and the accuracy of both estimated orbit and clock will be improved. As a result, the performance of PPP validation will be more prominent.

Discussion and conclusions

This study initially validates the potential for generating high-precision GPS orbit and clock products by integrating the measurements from a regional network and LEO satellites. The orbit accuracy of GPS satellites in the R, T and N directions is 2.27 cm, 3.45 cm, and 3.08 cm,

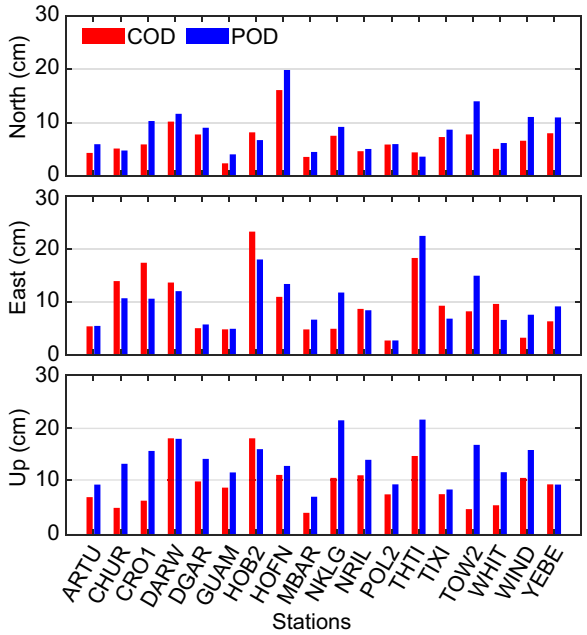

Fig. 15 Positioning accuracy of kinematic PPP based on COD final products and integrated POD products

Table 7 RMS values of kinematic PPP solutions based on COD and POD products (unit: cm)

Products	N	E	U
COD	6.72	9.37	9.38
POD	8.42	9.77	13.57

respectively, with the clock accuracy better than 0.15 ns. The LEO orbit accuracy is better than 2 cm in the R direction, and the position errors are mostly within 4 cm. Then based on the integrated POD products, kinematic PPP validation was carried out in terms of convergence time and positioning accuracy. Additionally, COD final products were utilized for comparative analysis. The results indicate that the PPP performance using POD products is generally inferior to that using COD products for most stations. This discrepancy is primarily attributed to larger orbit and clock errors in POD products compared to COD products. Moreover, the periods of missing observations can lead to the discontinuities in clock estimation. While it is evident that high precision GNSS orbits and clocks can be obtained by integrating the observations from regional stations and LEO satellites, it is important to note that the integrated solutions exhibit slightly lower accuracy in GNSS orbit, LEO orbit, and PPP performance compared to the solutions generated with the measurements of a well-distributed global network. Future efforts will focus on enhancing performance with ambiguity resolution and increased involvement of LEO satellites.

Acknowledgements
The authors are very grateful to GFZ for providing the GRACE-FO onboard GPS data and precise orbits, ESA for providing SWARM-A/B/C and Sentinel-3A/B onboard GPS data and precise orbits, AVISO for providing Jason-3 onboard GPS data and precise orbits, CODE for providing the GNSS final orbit and clock products, and IGS for providing ground station data and coordinates. We also want to thank the Net_Diff software published at http://202.127.29.4/shao_gnss_ac/ for providing the PPP validation.

Author contributions
S.Z. and X.H. provided the initial idea and the software for this study. K.L. and C.T. designed and performed the data analysis. X.Z. provided the LEO onboard data and reference orbits. X.Z. performed the POD of SAT-A/B/C/D/E based on the two-step method. K.L. wrote the manuscript. and C.T. helped improve the English. C.T., S.Z., X.H. and X.Z. helped improve the manuscript. All authors reviewed the manuscript.

Funding
This research is sponsored by the National Natural Science Foundation of China (Grant No. 12103077; Grant No. 12173072).

Availability of data and materials
The GPS final orbit and clock products are published and available from ftp://ftp.aiub.unibe.ch/CODE/. The onboard GPS data and precise orbits of GRACE-FO can be obtained from ftp://isdcftp.gfz-potsdam.de/grace-fo/Level-1A/JPL/INSTRUMENT/RL04/2019/. The onboard GPS data and precise orbits of SWARM-A/B/C are available from ftp:// swarm-diss.eo.esa.int /Level1b/Entire_mission_data/. The onboard GPS data and precise orbits Sentinel-3A/B are provided by ESA at https://scihub.copernicus.eu/dhus/#/home. The onboard GPS data and precise orbits of Jason-3 can be found at ftp:// ftp-access.aviso.altimetry.fr /geophysical-data-record/doris/jason-3/. The observation data and coordinates of IGS stations are provided at ftp://igs.ign.fr. The other data that support this study are available from the corresponding author upon reasonable request.

Declarations

Competing interests
The authors have no known conflicts of interest to declare.

Received: 11 July 2023 Accepted: 30 May 2024
Published online: 12 August 2024

References

Arnold, D., Meindl, M., Beutler, G., Dach, R., Schaer, S., Lutz, S., Prange, L., Sośnica, K., Mervart, L., & Jäggi, A. (2015). CODE's new solar radiation pressure model for GNSS orbit determination. *Journal of Geodesy, 89*(8), 775–791.

Berger, C., Biancale, R., Ill, M., & Barlier, F. (1998). Improvement of the empirical thermospheric model DTM: DTM94–a comparative review of various temporal variations and prospects in space geodesy applications. *Journal of Geodesy, 72*(3), 161–178. https://doi.org/10.1007/s001900050158

Blewitt, G. (1990). An automatic editing algorithm for GPS data. *Geophysical Research Letters, 17*, 199–202.

Boehm, J., Werl, B., & Schuh, H. (2006). Troposphere mapping functions for GPS and very long baseline interferometry from European Centre for Medium-Range Weather Forecasts operational analysis data. *Journal of Geophysical Research: Solid Earth, 111*(B2), B02406.

Boomkamp, H., & Dow, J. (2005). Use of double difference observations in combined orbit solutions for LEO and GPS satellites. *Advances in Space Research, 36*(3), 382–391.

Couderc, V. (2015). *Jason-3 characteristics for POD processing*. Technical report.

Duan, B., & Hugentobler, U. (2021). Comparisons of CODE and CNES/CLS GPS satellite bias products and applications in Sentinel-3 satellite precise orbit determination. *GPS Solutions, 25*(4), 128.
Fernández Martìn, C. (2016). Sentinel-3 properties for GPS POD, GMV-GMES-POD-TN-0027, v1.2.
Folkner, W., Williams, J., Boggs, D., Park, R., & Kuchynka, P. (2014). The planetary and lunar ephemerides DE430 and DE431. *Interplanetary Network Progress Report, 196*(1), 42–196.
Fossa, C., Raines, R., Gunsch, G., & Temple, M. (1998) An overview of the IRIDIUM (R) low Earth orbit (LEO) satellite system. In *Proceedings of the IEEE 1998 national aerospace and electronics conference. NAECON 1998. Celebrating 50 Years (Cat. No. 98CH36185)* (pp 152–159). https://doi.org/10.1109/NAECON.1998.710110
Geng, J., Shi, C., Zhao, Q., Ge, M., & Liu, J. (2008). Integrated adjustment of LEO and GPS in precision orbit determination. In *VI Hotine-Marussi symposium on theoretical and computational geodesy* (pp. 133–137). Berlin, Heidelberg: Springer.
He, M., Zhu, W., Feng, C., Huang, C., & Chang, H. (1988). SHORDE I program system and applications. *Celestial Mechanics, 45*, 61–64.
Huang, W., Männel, B., Sakic, P., Ge, M., & Schuh, H. (2020). Integrated processing of ground-and space-based GPS observations: Improving GPS satellite orbits observed with sparse ground networks. *Journal of Geodesy, 94*(10), 1–13.
Hugentobler, U., Jäggi, A., Schaer, S., & Beutler, G. (2005). Combined processing of GPS data from ground station and LEO receivers in a global solution. In Sansó F (ed) *A Window on the Future of Geodesy* (pp 169-174). Berlin, Heidelberg: Springer.
Jiang, K., Li, W., Li, M., et al. (2023). Precise orbit determination of Haiyang-2D using onboard BDS-3 B1C/B2a observations with ambiguity resolution. *Satellite Navigation, 4*, 28. https://doi.org/10.1186/s43020-023-00118-1
Johnston, G., Riddell, A., & Hausler, G. (2017). The international gnss service. In P. J. G. Teunissen & O. Montenbruck (Eds.), *Springer handbook of global navigation satellite systems* (1st ed., pp. 967–982). Cham: Springer. https://doi.org/10.1007/978-3-319-42928-1
Kang, Z., Bettadpur, S., Nagel, P., Save, H., Poole, S., & Pie, N. (2020). GRACE-FO precise orbit determination and gravity recovery. *Journal of Geodesy, 94*, 1–17.
Khalife, J., Neinavaie, M., & Kassas, Z. (2021). The first carrier phase tracking and positioning results with Starlink LEO satellite signals. *IEEE Transactions on Aerospace and Electronic Systems, 58*(2), 1487–1491. https://doi.org/10.1109/TAES.2021.3113880
König, R., Reigber, C., & Zhu, S. (2005). Dynamic model orbits and Earth system parameters from combined GPS and LEO data. *Advances in Space Research, 36*(3), 431–437.
Kouba, J. (2004). Improved relativistic transformations in GPS. *GPS Solutions, 8*(3), 170–180.
Li, K., Zhou, X., Guo, N., & Zhou, S. (2022b). Effect of PCV and attitude on the precise orbit determination of Jason-3 satellite. *Journal of Applied Geodesy, 16*(2), 143–150.
Li, X., Wang, Q., Wu, J., Yuan, Y., Xiong, Y., Gong, X., & Wu, Z. (2022a). Multi-GNSS products and services at iGMAS Wuhan Innovation Application Center: Strategy and evaluation. *Satellite Navigation, 3*(1), 1–19.
Li, X., Zhang, K., Zhang, Q., Zhang, W., Yuan, Y., & Li, X. (2018). Integrated orbit determination of FengYun-3C, BDS, and GPS satellites. *Journal of Geophysical Research: Solid Earth, 123*(9), 8143–8160.
Lyard, F., Lefevre, F., Letellier, T., & Francis, O. (2006). Modelling the global ocean tides: Modern insights from FES2004. *Ocean Dynamics, 56*(5–6), 394–415.
Männel, B., & Rothacher, M. (2017). Geocenter variations derived from a combined processing of LEO-and ground-based GPS observations. *Journal of Geodesy, 91*(8), 933–944.
Montenbruck, O., Gill, E., & Lutze, F. (2002). Satellite orbits: Models, methods, and applications. *Springer, Heidelberg*. https://doi.org/10.1115/1.1451162
Osoro, O., & Oughton, E. (2021). A techno-economic framework for satellite networks applied to low earth orbit constellations: Assessing Starlink, OneWeb and Kuiper. *IEEE Access, 9*, 141611–141625. https://doi.org/10.1109/ACCESS.2021.3119634
Pavlis, N., Holmes, S., Kenyon, S., & Factor, J. (2012). The development and evaluation of the Earth Gravitational Model 2008 (EGM2008). *Journal of Geophysical Research: Solid Earth, 117*(B4), B04406.
Petit, G,. Luzum, B.: IERS Conventions (2010), IERS Technical Note No. 36 (Verlag des Bundesamts für Kartographie und Geodäsie, Frankfurt 2010).
Reid, T., Neish, A., Walter, T., & Enge, P. (2016). Leveraging commercial broadband leo constellations for navigating. In *Proceedings of the ION GNSS+ 2016, Institute of Navigation, Portland, Oregon, USA*, September 12–16 (pp 2300–2314).
Reid, T., Neish, A., Walter, T., & Enge, P. (2018). Broadband LEO constellations for navigation. *Navigation, 65*(2), 205–220. https://doi.org/10.1002/navi.234
Rodriguez-Solano, C., Hugentobler, U., Steigenberger, P., & Lutz, S. (2012). Impact of Earth radiation pressure on GPS position estimates. *Journal of Geodesy, 86*(5), 309–317.
Saastamoinen, J. (1972). Contributions to the theory of atmospheric refraction. *Bulletin Géodésique (1946–1975), 105*(1), 279–298.
Schmid, R., Steigenberger, P., Gendt, G., Ge, M., & Rothacher, M. (2007). Generation of a consistent absolute phase-center correction model for GPS receiver and satellite antennas. *Journal of Geodesy, 81*(12), 781–798.
Siemes, C. (2019). *Swarm instrument positions related to GPS receiver data processing*. Technical report, RHEA for ESA, ESA-EOPSM-SWRM-TN-3559.
Tang, C., Hu, X., Zhou, S., Liu, L., Pan, J., Chen, L., Guo, R., Zhu, L., Hu, G., Li, X., & He, F. (2018). Initial results of centralized autonomous orbit determination of the new-generation BDS satellites with inter-satellite link measurements. *Journal of Geodesy, 92*, 1155–1169.
Tapley, B., Ries, J., Davis, G., Eanes, R., Schutz, B., Shum, C., Watkins, M., Marshall, J., Nerem, R., Putney, B., Klosko, S., Luthcke, S., Pavlis, D., Williamson, R., & Zelensky, N. (1994). Precision orbit determination for TOPEX/POSEIDON. *Journal of Geophysical Research: Oceans, 99*(C12), 24383–24404.
van den Ijssel, J., Encarnação, J., Doornbos, E., & Visser, P. (2015). Precise science orbits for the Swarm satellite constellation. *Advances in Space Research, 56*(6), 1042–1055.
Yang, L. (2019). The centispace-1: A LEO satellite-based augmentation system. In *14th Meeting of the International Committee on Global Navigation Satellite Systems, Bangalore, India*, December 9–13.
Yang, Y., Mao, Y., Ren, X., Jia, X., & Sun, B. (2024). Demand and key technology for a LEO constellation as augmentation of satellite navigation systems. *Satellite Navigation*. https://doi.org/10.1186/s43020-024-00133-w
Yang, Y., Yang, Y., Hu, X., Chen, J., Guo, R., Zhou, S., Zhao, L., & Xu, J. (2020). Inter-satellite link enhanced orbit determination for BeiDou-3. *The Journal of Navigation, 73*(1), 115–130. https://doi.org/10.1017/S0373463319000523
Ye, S. (2002). Theory and its realization of GPS precise point positioning using un-differenced phase observations . PhD Dissertation, GNSS Research Center, Wuhan University.
Zhang, K., Li, X., Wu, J., Yuan, Y., Li, X., Zhang, X., & Zhang, W. (2021). Precise orbit determination for LEO satellites with ambiguity resolution: Improvement and comparison. *Journal of Geophysical Research Solid Earth, 126*(9), e2021JB022491. https://doi.org/10.1029/2021jb022491
Zhao, Q., Wang, C., Guo, J., Yang, G., Liao, M., Ma, H., & Liu, J. (2017). Enhanced orbit determination for BeiDou satellites with FengYun-3C onboard GNSS data. *GPS Solutions, 21*(3), 1179–1190.
Zhu, S., Reigber, C., & König, R. (2004). Integrated adjustment of CHAMP, GRACE, and GPS data. *Journal of Geodesy, 78*(1), 103–108.
Zoulida, M., Pollet, A., Coulot, D., Perosanz, F., Loyer, S., Biancale, R., & Rebischung, P. (2016). Multi-technique combination of space geodesy observations: Impact of the Jason-2 satellite on the GPS satellite orbits estimation. *Advances in Space Research, 58*(7), 1376–1389.

Publisher's Note